ULTRASONIC IMAGING 11, 42-74, (1989)

NUMERICAL STUDY OF HIGHER-ORDER DIFFRACTION TOMOGRAPHY VIA THE SINC BASIS MOMENT METHOD

Thomas J. Cavicchi[1] and William D. O'Brien, Jr.[2]

Bioacoustics Research Laboratory
Department of Electrical and Computer Engineering
University of Illinois
1406 W. Green Street
Urbana, IL 61801

Behavior and limitations of the sinc basis method have been discovered during simulation studies. An iterative row-action method (ART) is compared with a full-matrix, least-squares solution (QR decomposition) and the problem of multiple solutions is discussed. Knowledge of the spatial distribution of scattered field energy can be used to speed up convergence. The first iteration is shown to be equivalent to the first Born solution. A fundamental limitation of present diffraction tomography algorithms, concerning phase shift through the scatterer, is found and related to clinical values. Effects of improvements on the initial guesses for the object function and internal field are studied. Lossy cylinder and contrived multicomponent reconstructions yield additional understanding of the phase shift problem. A sequence of simulations investigates estimated solution movement in hyperspace.

Key words: Diffraction tomography; high-order inverse scattering; moment method; integrated phase shift.

1. INTRODUCTION

To obtain high-resolution quantitative images of acoustic quantities (such as sound speed and absorption coefficient) in tissue from measurements of the interaction of ultrasound waves with tissue, diffraction effects must be included. This is true at diagnostic frequencies because the wavelength is of the same order as the sizes and spacings of the scatterers throughout the soft tissue to be imaged [1]. Essentially all previous ultrasonic diffraction tomography algorithms [2] depend on first-order scattering assumptions for their validity, conditions which do not hold in

---

[1]Current address: Electrical Engineering Department, University of Akron, Akron, OH 44325.

[2]Author to whom correspondence should be addressed.

0161-7346/89 $3.00

practical tissue inverse scattering problems. (For example, under the first Born approximation, the total field is assumed to be equal to the incident field. Under the Rytov approximation, the second-order quantity $[\nabla\psi'(\vec{r})]^2$ is ignored, where $\psi'(\vec{r})$ is the complex phase shift between the total and incident fields [4].)

Independent investigations of the sinc basis moment method have been carried out [3], exploring the behavior of this method under a variety of conditions of scattering object quantities and algorithm parameters. A summary of the pertinent theory appears in [3]. That study as well as the present work focused on computer simulation reconstructions of infinite circular cylinders of varying size and speed of sound. The scattering cylinder, in a homogeneous coupling medium, is exposed to simulated cylindrical ultrasonic waves. The shape of a circular cylinder was chosen because a series solution of the forward scattering problem is available, allowing independent verification of the solution of the inverse scattering problem yielded by this algorithm. Relaxation constants, grid size, and sampling density were among the algorithm parameters varied in that earlier work.

Because of the computational limitations at that time (a VAX 11/730 was used), the maximum sizes of the scatterers were restricted to only one or two wavelengths. Access to an Alliant FX/8 minisupercomputer has made possible a greater understanding of the conditions for accurate reconstructions, and provides a window into the behavior of the algorithm (e.g., speed and accuracy) for larger object sizes. (This machine has a UNIX operating system, virtual memory, eight 64-bit floating-point processors, fast interprocessor synchronization, and vector instructions. Each processor (Computational Element) can run at 12 megaflops peak (so 96 total). The capacity of memory is 64 megabytes.)

In particular, a major problem identified using the super computer was the existence of multiple local solutions; the iterative (perturbation) form of the algorithm settles on the closest local solution. When the closest local solution is the desired solution, perturbation methods can be said to succeed. But two converse cases show the difficulty arising from local solutions. First, a full matrix solution (QR decomposition) yields a solution far away from that desired because of a discretization error in the scattered field equations. In that case, the closest local solution was desired, but not obtained. Second, for problems in which the magnitude of the phase shift through the object exceeds π, the perturbation methods fail by settling on an erroneous solution close to zero phase shift (the case of a homogeneous medium, which is the starting point); in these cases, the closest local solution is not the one desired but is the one obtained.

2. QR DECOMPOSITION

The iterative method ART [3] is a perturbation method for solving the nonlinear tomographic matrix equations resulting from the sinc basis formulation. It converges to a local solution close to the initial guess (typically zero) for the desired object function. For a mathematical characterization of ART, see [4]. It was desired to see what would be the result of a full matrix least squares solution of the scattered field matrix equations, as opposed to the row-at-a-time operation of ART; QR decomposition was chosen. For a mathematical description of QR decomposition applied to least squares problems, see [4] or [5].

The effect of this method of solution on the reconstructions is now examined. A 17x17 grid was used to reconstruct a $k_o a = 10$ cylinder for which the speed of sound, c_1, was 5 percent above c_o, the homogeneous

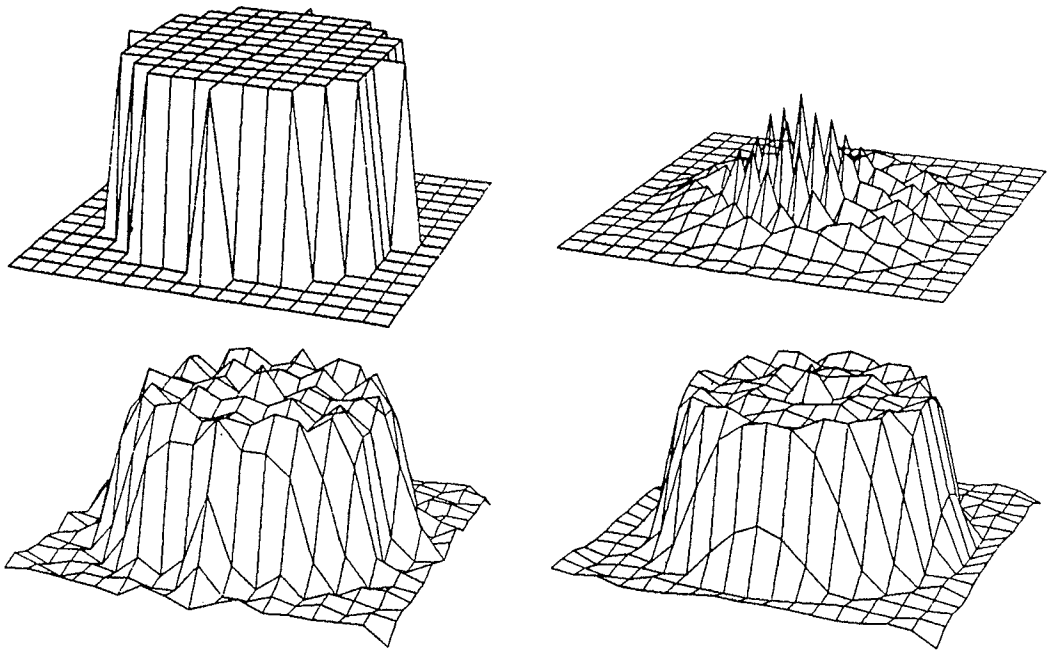

Fig. 1 Speed of sound reconstructions for lossless, $k_o a = 10$, 5 percent speed of sound mismatch cylinder using QR decomposition (above) and ART (below). Scattered field was generated by the sinc basis expansion equations in forward mode (left) and by the exact series solution (right).

medium speed of sound. Figure 1 shows the first iteration speed of sound reconstructions for four cases. In the upper row are reconstructions using the routine SQRST (QR decomposition) from the Linpack software package to solve the scattered field equations for an estimate of the object function, and in the bottom row are corresponding first iteration reconstructions made under the same conditions but calculated via the ART. Define γ^{ex} to be the exact object inhomogeneity function [3] and γ^{QR} to be the solution for the object function by QR decomposition. To eliminate one source of error, the exact internal field [6] was used for all these reconstructions. On the left column reconstructions, this exact field was substituted along with γ^{ex} into the scattered field equations to generate the scattered field data, rather than using the exact series solution as is usually done [3]. Because the scattered field data were generated by the same equations as are used for reconstruction, the data are a perfect match, and $\gamma^{QR} \simeq \gamma^{ex}$ as shown in the upper left reconstruction. But if the exact scattered field [6] is used (reconstructions on the right) the solution by QR decomposition is poor; the reconstructed speed of sound in the cylinder region of that reconstruction actually dips below c_o. The reason for the discrepancy is the sinc basis discretization error, which embodies among other approximations, the assumption the γf is bandlimited, where f is the total pressure field. Using ART with scattered field data generated by the sinc basis scattered field equations, the reconstruction (lower left) is essentially

identical to that obtained for the case of using exact scattered field values (lower right). The reason appears to be that in ART one can and does take advantage of the knowledge that $||\gamma||$ is small, and evidently γ^{ex} or, rather, a vector near γ^{ex}, is the smallest local solution of the scattered field equations using exact scattered field data; whereas QR decomposition can make no use of such prior information. The full matrix solution can, however, be "regularized" by additional computations involved in an augmentation of the intitial matrix equation: $\epsilon\gamma = 0$, where ϵ is an empirically determined constant. Indeed, γ^{QR} has a norm sixty times greater than that of γ^{ex}. The normalized inner product of γ^{QR} with γ^{ex} is only about 0.3.

One could view the mismatched scattered field case as equivalently an addition of noise to the original least squares inversion, with respect to $q^{\epsilon\chi}$; however, it is noiseless with respect to γ^{QR}. In ART, when $\tilde{\gamma}^o = \gamma^{QR}$, the iterated $\tilde{\gamma}$ does not move away from γ^{QR}. Because $\tilde{\gamma}^o$ can be placed wherever it is desired, there is somewhat greater flexibility with ART than with QR decomposition. Also, as an iterative technique, far fewer calculations are necessary (due to using the increasingly better "initial" guess) than for solving the entire matrix problem repeatedly. For QR decomposition, all that can be done is to make the assumption that $||\gamma||$ is small by selection of a problem-dependent augmentation of the matrix equation mentioned above (for which in one problem $\epsilon = 10^{-5}$ worked well). In ART, the only way γ is constrained to be small is by way of the initial guess $\tilde{\gamma}^o = 0$, which influences which local minimum will be obtained. In principle, one could choose $||\tilde{\gamma}^o||$ to be as large as desired. However, that would violate the assumption that $||\gamma^{ex}||$ is small, which is inherent in the sinc basis formulation and alternating variables solution procedure (independent of how the intermediate matrix equations are solved).

One may argue that ART will provide a "regularized" solution only if the number of iterations is sufficiently small, and that $\tilde{\gamma}$ will eventually move to γ^{QR}. Empirically, this has been shown to be false. For a unity relaxation constant in the scattered field equations (no under-relaxation, which is a worst case for bad data) and a 5 percent speed of sound contrast cylinder, ART was allowed to iterate 75 times on only the mismatched scattered field equations. After rapidly hitting a minimum the error eventually increased by only < 0.1 percent of $||\gamma^{ex}||^2$, and the decreasing increments were finally about 0.001 percent per iteration; for all practical purposes ART had settled on a good local solution.

It should be mentioned that there is an additional significance of the study of γ^{QR}: γ^{QR} is the result of imperfect measurements on a noniterative, unregularized· least squares solution, as hinted above. The condition number for the scattered field equations matrix is on the order of hundreds; as a result, small measurement errors in f^{sc} cause large errors in $\tilde{\gamma}$. Results in Section 13 below compare the behavior of $\tilde{\gamma}$ by ART with both γ^{ex} and the solution of the perturbed equation, γ^{QR}. Through simulations, it is empirically verified that γ^{ex} is a local solution of the perturbed equation, while γ^{QR} is its true solution. Thus, ART is relatively insensitive to errors in the scattered field measurements.

Another problem with using QR decomposition is the order of storage (n^5 compared with n^3 for ART for an nxn image) and the overall order of computation, which for this algorithm appears to be n^7 compared with n^4 for ART using the FFT for the internal field equations [7]. For example, on the supercomputer the decomposition time for the 25x25 case was about 25 minutes, and would have to be done many times over a complete iteration (including decomposition of the internal field equations matrices). When compared with 33 seconds for four complete iterations using ART, there is no contest. However, the unfortunate appearance of multiple solutions

apparently arising from the bandlimited and discretized representations of full-band, continuous integrals and functions remains, and warrants reexamination of the numerical techniques in order to understand and ultimately overcome this limitation.

3. EFFECT OF DISTRIBUTION OF SCATTERED FIELD ENERGY

One helpful way of characterizing performance is to examine the variation in absolute value of the error in the estimated scattered field values vs. increasing row correction number i. First, figure 2 shows the magnitude squared of the scattered field for views 1 and 10 for n = 25, number of transmitters n_{trans} = 40, number of detectors n_{det} = 32: a $k_o a$ = 12.6, 16 percent speed of sound contrast cylinder. Let i_{det} = i modulo (n_{det}). Notice that the peaks occur at approximately $i_{det} = 17 = n_{det}/2 + 1$ and $i_{det} = 24 = [9 \cdot n_{det}/n_{trans}] + n_{det}/2 + 1$ (where [] indicate a greatest integer operation) because that receiver is opposite the transmitter. Also notice how narrow the distribution is about its center. (The slight asymmetries about the center are due to unequal n_{det} and n_{trans} values, causing the sampling angles to be not necessarily symmetrical about the center of the distribution.)

Now consider figure 3: for -6 percent speed of sound contrast and $k_o a$ = 12.6, the absolute value of the error in the estimated scattered field is shown for the first 128 rows of iteration 1. Notice that the peaks are 32 = n_{det} rows apart, and occur for i_{det} on the point on the ring

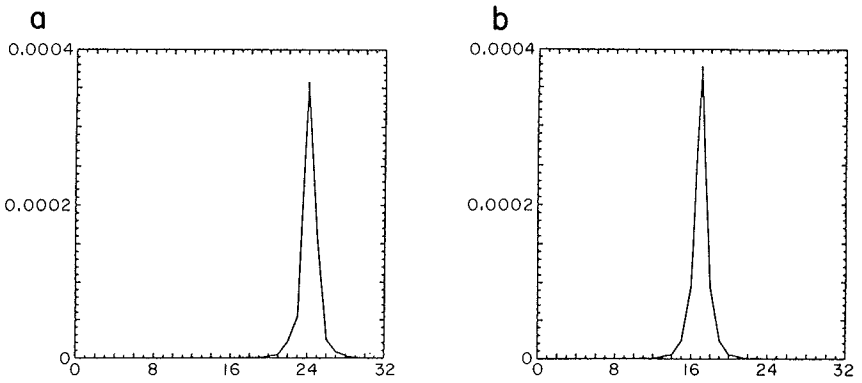

Fig. 2 $|f^{sc}(1,i_{det})|^2$ (a) and $|f^{sc}(10,i_{det})|^2$ (b) vs. receiver i_{det}, where $f^{sc}(j,i_{det})$ = the exact scattered acoustic field from a circular cylinder insonified by a unit amplitude cylindrical wave originating at transmitter j and measured at receiver i_{det}. All transducers are on a circular ring of radius 100λ from the cylinder center. The peak occurs at the point opposite on the ring of transducers from the transmitter, so increasing the viewing angle merely shifts the maximum; the peak location is approximately where $i_{det} = [(j-1)n_{det}/n_{trans}] + n_{det}/2+1$, and here [] indicates a greatest integer operation.

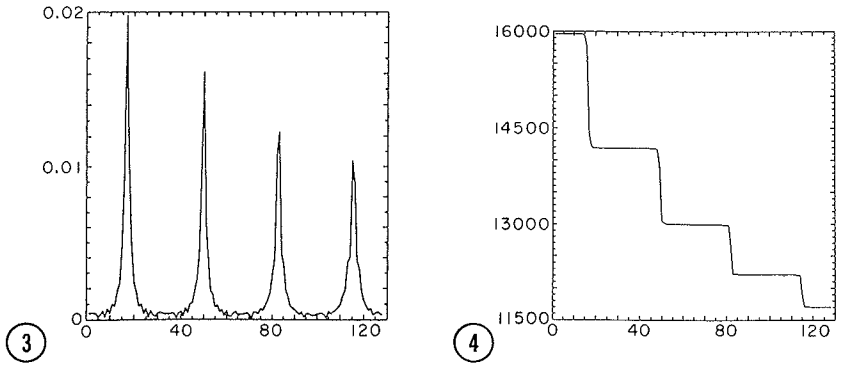

Fig. 3 Absolute value of the error in estimated scattered field vs. row of correction via ART for the first 128 corrections of iteration 1 ($k_o a = 12.6$, $c_1 = 1.7391$ mm/μs).

Fig. 4. Squared error in $\tilde{\gamma}$, $\Sigma(\tilde{\gamma}_j - \gamma_j^{ex})^2$, vs. row of correction (in scattered field matrix equations) for the first 128 rows of iteration 1 of a reconstruction of a $k_o a = 12.6$, $c_1 = 1.4118$ mm/μs cylinder.

of transducers opposite the transmitter, where the scattered field energy is maximum (as in figure 2). The four peaks represent the first four views of correction to $\tilde{\gamma}$. For the first view especially, the shape of the peak is close to that of the scattered field distribution shown in figure 2 (though not here squared) because the estimated object function $\tilde{\gamma} \simeq 0$ and the error in the estimated scattered field approximately equals the scattered field; it is maximum at $i_{det} = n_{det}/2 + 1 = 17$.

Such plots as in figure 3 can help, along with those of squared error in $\tilde{\gamma}$ vs. row of correction in determining the optimal sequence of iterative correction on $\tilde{\gamma}$. Based on the above observations, the behavior in figure 4 can be understood. Figure 4 is a plot of the squared error in $\tilde{\gamma}$ vs. row of correction for the first 128 rows of iteration 1 of the same reconstruction. Immediately it is evident that the big jumps occur $32 = n_{det}$ rows apart and coincide with the regions of maximum scattered field energy (because the initial scattered field error is greater, causing greater corrections to be made to $\tilde{\gamma}$). It appears that by correcting $\tilde{\gamma}$ using first these rows of maximum scattered field energy, the convergence can be speeded up.

Figure 5 illustrates the advantage of using this idea. Shown are squared errors in $\tilde{\gamma}$ for all 1280 rows of iteration 1. In the left figure, normal numerical row order was used for the iterative corrections. The small jumps again indicate corrections occurring for rows of maximum scattered field energy. The right figure shows the same errors in $\tilde{\gamma}$, but ordering the rows of correction so that the rows corresponding to the receivers measuring maximum scattered field energy are used first in correcting $\tilde{\gamma}$, and then the others. In this example, defining

$$i_p = 1 + n_{det}\left[\frac{(i_{trans}-1)}{n_{trans}} + \frac{1}{2}\right] \qquad (1)$$

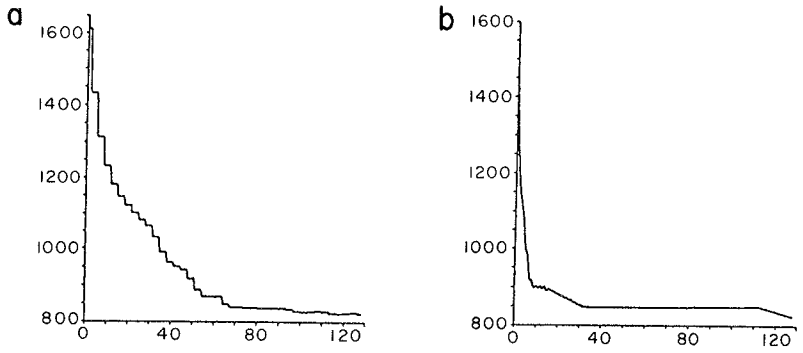

Fig. 5 Squared error in $\tilde{\gamma}$ vs. row correction for each row of correction in iteration 1 reconstruction of a $k_o a = 12.6$, $c_1 = 1.4117$ mm/μs cylinder. On the left, normal ordering of rows was used; on the right, the rows are ordered according to Eq. (1) and surrounding discussion. The result is a four to five factor of increase in convergence speed from the left column to the right column.

then the following sequence is used: view by view, beginning with $i_{trans} = 1$, only receivers $i_p - 1$ through $i_p + 1$ are used, for all views; then the other receivers. A dramatic increase in speed over the left figure is evident; about a fivefold decrease occurred in the number of corrections it took to reach nearly the final value of $\tilde{\gamma}$ for the iteration. For the general case, a simple, quick determination of the receivers with maximum scattered field energy could be used to implement this idea for a practical application, given that the other problems of practicality of the sinc basis method discussed in this paper could be solved. Using this idea, significant underdetermination, with its advantages of resulting speed and practicality, may be possible without large adverse affects on the reconstruction accuracy.

4. COMPARISON OF FIRST ITERATION OF SINC BASIS METHOD WITH FIRST-ORDER DIFFRACTION TOMOGRAPHY SOLUTION

To relate performance of the sinc basis method to other existing algorithms, a comparison study was done between the sinc basis moment method and a representative first-order diffraction tomography algorithm based on the Born approximation and implemented by several researchers (for example [8] and [9]). In the Fourier Diffraction Theorem used in the first-order Born solution, the Green function is expanded over an angular spectrum. That expansion is substituted into the integral equation for the scattered field. The coefficients of the resulting angular spectrum representation of the scattered field are directly expressible in terms of the Fourier transform of the field evaluated on a convenient surface outside the object region. If now the incident plane wave field is substituted as an approximation of the total field under this integral and the result is identified as the complex scattered field, the first Born approximation has been made. And with this substitution a second identification of the angular spectrum coefficients can be made: they are values on a semicircular arc of the Fourier transform of the object function. (Had the substitution of the

incident field for the total field not been made, these coefficients would represent Fourier transform values of the object function times the total, unknown field, and no intrinsic property of the medium could then be ascertained.) A diffraction tomography simulation program based on the above formulation using the first Born approximation (as opposed to the Rytov approximation, which can also be used in the above theory to obtain a diffraction tomography algorithm) was implemented on the VAX 11/730 computer. Signal processing details of [9] were followed.

It is obvious that this Fourier domain interpolation and inversion technique has very little in common computationally with the sinc basis moment method, where closed-form integrations of quadruple sinc functions, matrices composed of elements having Hankel function sample values and numerical integrations of Bessel functions times double sinc functions as factors, and underrelaxed iterative orthogonal projections using these matrices combine into a complex procedure alien to the Fourier Diffraction Theorem [4]. Furthermore, the measurement geometry was quite different: the Fourier Diffraction Theorem in its commonly stated form requires the receivers to be on a line in front of (reflection mode) or behind (transmission mode) the scattering object, and they must be spaced closely enough to satisfy a Nyquist criterion. For the sinc basis moment method, receivers can be placed on any surface outside the object region, and there are no spacing requirements on these measurements, for no discrete Fourier transforms are taken of the received signals. Figure 6 shows center line profiles of speed of sound and absorption reconstructions of $k_o a = 12.6$ lossless cylinders for three contrast values: -10, 5, and 13.3 percent. The first iteration of the sinc basis moment method and the Fourier Diffraction Theorem are in all cases the curves very close together; the other two curves are the fourth iteration of the sinc basis method and the exact solution (straight lines). For the weak scattering case a remarkable improvement over the first-order reconstructions is evident. For this comparison study the receivers were placed on a line perpendicular to the direction of the incident wave and behind the object region in the Fourier Diffraction Theorem algorithm, and on a circular ring around the object region in the sinc basis algorithm. The only things kept in common between uses of the two methods were the object region grid spacings, the distance from the receiver line to the center of the object region in the Fourier domain method and the radius of the ring of detectors in the sinc basis method, the incident fields, the object functions being reconstructed, and the use of the Born approximation in the integral equation for the scattered field. The common use of the Born approximation is the cause for the astounding agreement between the two solutions for both low and high magnitude, positive and negative contrast cases. What is most amazing is that both first-order reconstructions fail in exactly the same way for the high contrast cases, where it is known that the Born approximation is not valid.

Table I provides further proof of similarity between the two solutions for the three cases examined above. Define $\gamma^{S.B.,1}$ to be the estimated object function after one iteration of the sinc basis moment method and $\gamma^{F.D.T.}$ to be the estimated object function resulting from the Born approximation mode of the Fourier Diffraction Theorem method. The complex normalized inner products between $\gamma^{S.B.,1}$ and γ^{ex}, $\gamma^{F.D.T.}$ and γ^{ex}, and $\gamma^{S.B.,1}$ and $\gamma^{F.D.T.}$ are given for the three contrast values. For the high contrast cases $\gamma^{S.B.,1}$ and $\gamma^{F.D.T.}$ are both far from one but nearly equal; moreover $\gamma^{S.B.,1} \cdot \gamma^{F.D.T.}$ is practically equal to one for all cases. This connection allows assessment of the sinc basis moment method and in particular gives strong credibility to a generalization of the applicability of conclusions to be made later using the error plots discussing first vs. higher iterations of the sinc basis method to the comparison of the Born approximation solution vs. higher iterations of the sinc basis method.

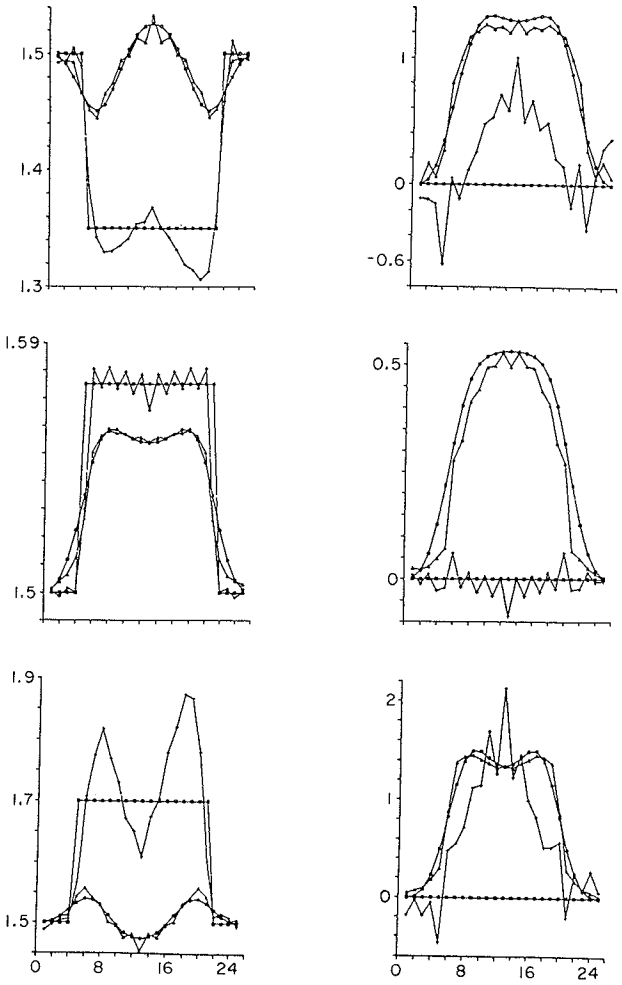

Fig. 6 Center-line profiles of first- and fourth-iteration speed of sound (left) and absorption (right) reconstructions and exact solutions for lossless $k_o a = 12.6$ cylinders. Variation in object reconstruction quality with speed of sound contrast: top to bottom, -10, 5, and 13.3 percent. Straight-line distribution is exact solution, two curves close together are (smoother line) Fourier Diffraction Theorem solution and the first iteration of the sinc basis moment method, and remaining curve is the fourth iteration of the sinc basis moment method.

5. OBJECT SIZE FOR LARGE OBJECTS

In this section, reconstructions of lossless, 5 percent speed of sound mismatch circular cylinders are presented for varied object size, ranging from $k_o a = 18$ to $k_o a = 32$.

Table I. Complex Normalized Inner Products Between $\gamma^{S.B.,1}$, $\gamma^{F.D.T.}$, and γ^{ex}

c_1, mm/μs / inner product	1.35	1.575	1.70
$\frac{\gamma^{S.B.,1}\ \gamma^{ex*}}{\|\|\gamma^{S.B.,1}\|\|\ \|\|\gamma^{ex*}\|\|}$	0.25+j0.87	0.82-j0.5	0.23-j0.88
$\frac{\gamma^{F.D.T.}\ \gamma^{ex}}{\|\|\gamma^{F.D.T.}\|\|\ \|\|\gamma^{ex*}\|\|}$	0.29+j0.85	0.78-j0.53	0.19-j0.90
$\frac{\gamma^{S.B.,1}\ \gamma^{F.D.T.}}{\|\|\gamma^{S.B.,1}\|\|\ \|\|\gamma^{F.D.T.}\|\|}$	0.99+j0.035	0.99+j0.014	0.99+j0.012

Iterations one and four are summarized and quantitatively compared with the exact solution in figure 7, which is a composite of speed of sound reconstructions. One can see that for small objects the first iteration (Born approximation) yields highly erroneous speed of sound and absorption values within the cylinder, while the fourth iteration is a dramatic improvement, oscillating closely about the exact solution values. But as the size increases to about $k_o a = 25$, even the sinc basis method begins to fail and become asymmetrical. This effect at first appears to be a numerical artifact of this implementation of the algorithm, occurring when conditions for the validity of the equations are only marginally satisfied. Because only the measured scattered field equations are used to generate the first iteration reconstruction, the symmetry present for all sizes isolates the origin of the problem as being in the other set of equations, the internal field equations. The position of the peak in the asymmetry has been shown to depend on the order of the viewing angles in the iterative correction within the internal field equations. It was thought that because most of the correction is done during whichever view is first considered, by underrelaxing the first few views relative to the others this effect might be reduced. However, for the first three views, changing the relaxation constant from 1.0 to 0.2 changed the detail in but not the degree of asymmetry.

6. PHASE SHIFT THROUGH THE OBJECT

At this point, it is helpful to define what is meant by "phase shift through the object." If a wave undergoes a phase change from ψ_0 to ψ_1 when travelling a distance R through free space (Fig. 8), and undergoes a

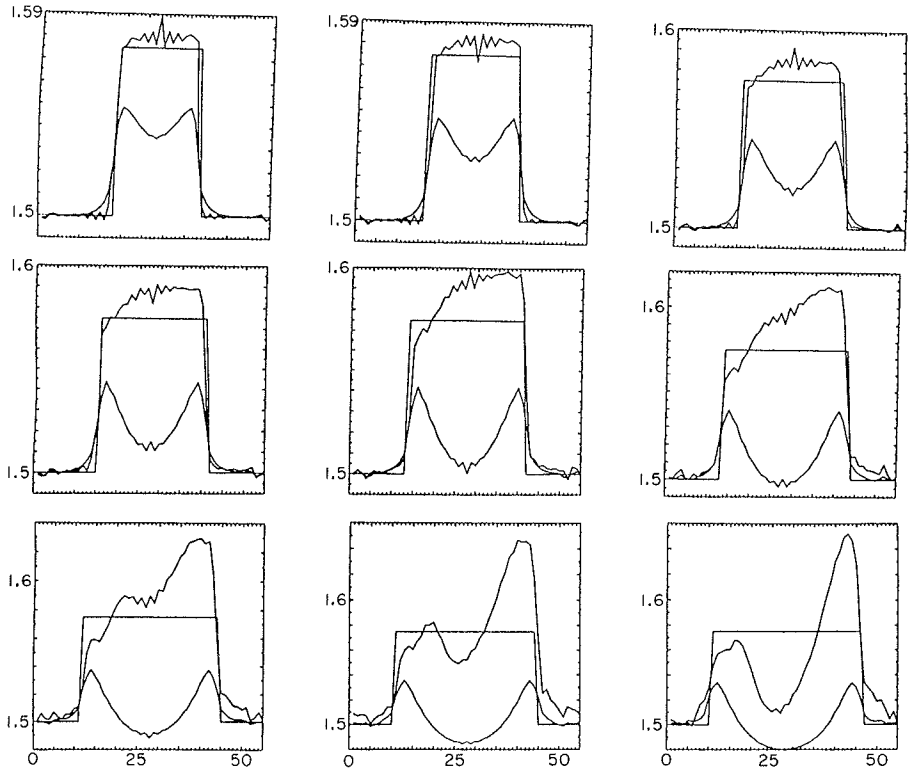

Fig. 7 Center-line profiles of first- and fourth-iteration speed of sound reconstructions and exact solution for lossless, 5 percent speed of sound mismatch cylinders. Variation in object reconstruction quality with object size. Left to right, top to bottom: $k_o a$ = 17.9, 19.7, 21.5, 23.3, 25.0, 26.8, 28.6, 30.4, and 32.2. Straight-line distribution is exact solution, symmetrical M-shaped curve is first iteration, and remaining curve is fourth iteration.

phase change from ψ_0 to ψ_2 when travelling the same distance, but in its course also passing through the diameter of a circular cylinder of different speed of sound, the difference in phase shifts is called $\Delta\psi$. That is,

$$\Delta\psi = \psi_2 - \psi_1 = \omega(2a)\left(\frac{1}{c_1} - \frac{1}{c_o}\right) \tag{2}$$

A fundamental problem arises from the periodicity in phase representations. The basic hypothesis is that when $|\Delta\psi|$ exceeds π, there will be information lost about it when sines and cosines are taken for the representation of the field during the reconstruction computations, resulting in a nonuniqueness of solution. Essentially, $2\pi + \pi/4$ becomes indistinguishable from $\pi/4$.

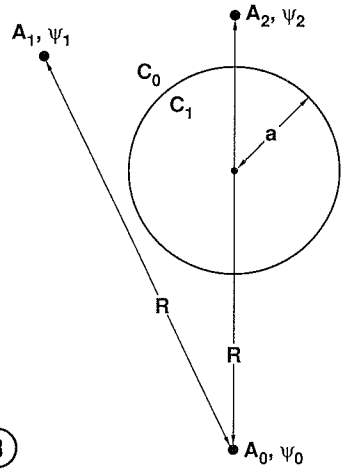

8

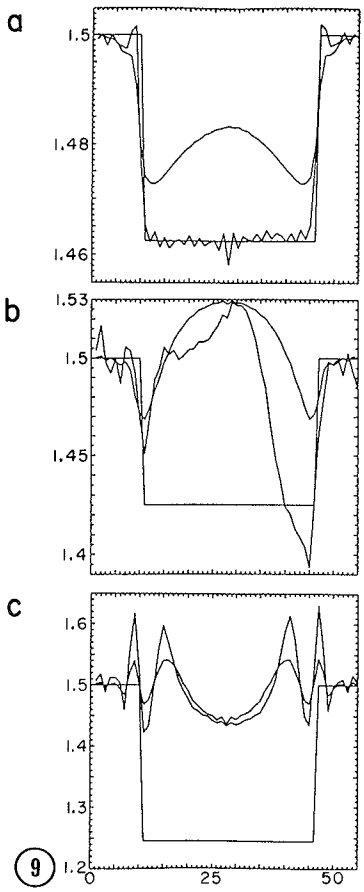

9

Fig. 8 Phase shift through a cylinder with speed of sound c_1 compared with equivalent propagation distance through homogeneous medium with speed of sound c_0. Originating signal has amplitude A_0 and phase ψ_0, signals a distance R away passing through homogeneous medium and through cylinder diameter have, respectively, amplitudes A_1 and A_2 and phase shifts ψ_1 and ψ_2. (If lossless medium, $A_1 = A_0$.)

Fig. 9 Center-line profiles of first- and fourth-iteration speed of sound reconstructions (and exact solution) for lossless, $k_0a = 32$ cylinders. Speed of sound contrast is -2.5 percent (a), -5 percent (b), and -17 percent (c); corresponding phase shifts are $\Delta\psi/\pi = 0.5$, 1.0, and 4.2. In (a), iteration four is that closer to the exact solution; in (b), iteration four is the asymmetrical curve; in (c), iteration four is the larger magnitude curve; the other curves are first iteration reconstructions.

In figure 4 of [3], an early study of the sinc basis method examining contrast variation for three small object sizes, the only case for which higher iterations were degradations rather than improvements over the lower

iterations was that for $k_o a = 13.6$, -10 percent contrast. It is also the only case in that entire composite for which $|\Delta\psi| > \pi$ ($\Delta\psi = 1.11\pi$).

In the object size study described above (Fig. 7), the phase shift ranged from $-\pi/2$ to $-\pi$. There one finds that, around $\Delta\psi = -0.87\pi$ (beginning of the third row of figure 7) reconstruction quality is already poor. In fact, it will be seen in the following study that often the sinc basis method fails slightly before $|\Delta\psi| = \pi$ is reached. This is probably due to the discretization and sinc basis expansion limitations on the representation of the various fields. However, the results of that object size study could have been made to appear somewhat more favorable and uniform by increasing the sampling density with decreasing cylinder size to maintain a constant sampling density to estimated Nyquist density (see [3]) but, because in general the object function (and consequently an accurate estimate of its bandwidth) is not known ahead of time, such an action seems unjustifiable. For this reason, the other of the two ways of varying the phase shift--varying the speed of sound contrast as opposed to object size (see Eq. (2))--produces results that are more easily and closely comparable. Details of speed of sound contrast studies for $k_o a = 32$ and $k_o a = 46$ studies, as well as many other miscellaneous studies and results, can be found in [4].

The behavior described above with respect to phase shifts is summarized concisely in figure 9. Shown there are speed of sound reconstructions for a $k_o a = 32$ cylinder for three contrast values: -2.5, -5, and -17 percent with corresponding phase shifts $\pi/2$, π, and 4.2π. For the low contrast object the fourth iteration shows dramatic improvement over the first iteration reconstruction. Significant asymmetry and loss of accuracy becomes evident for the medium contrast object (in the vicinity of π). Symmetry returns for high contrast, but the (stable) solution is erroneous.

The reconstruction does not blow up, oscillate, or randomly wander, but settles on an erroneous solution. That supports the hypothesis that above π, there is a nonuniqueness phenomenon taking the iterated solution away from that desired and along the path of a solution with phase shift magnitude less than π. The phase shifts through reconstructed cylinders having true phase shifts greater than π were calculated as follows:

$$\hat{\Delta\psi} = \omega h \sum_{i=1}^{n} \left(\frac{1}{\tilde{c}_i} - \frac{1}{c_o} \right) \tag{3}$$

where h is the spatial sample spacing, $\hat{\Delta\psi}$ is the estimated phase shift through a midline of the object region, and $\tilde{c}_i$ is the speed of sound estimate for pixel $(i_x, i_y) = (i, n/2 + 1)$. Almost invariably, the phase shifts were of magnitude less than π. Perhaps it is this retracking of the solution that may account for the subtle artifact of asymmetry that occurs only in the vicinity of $\pm\pi$.

One might ask if the reconstructed phase shift in some way follows the correct phase shift, modulo π. This possibility was investigated for $k_o a = 12.6$ cylinders. It was found [4] that there was no discernable pattern, such as a strong correlation with $\hat{\Delta\psi} = \Delta\psi$ modulo(π). The situation is more complicated than a characterization of the sinc basis method as being simply a means of reconstructing phase shifts (e.g., many signals of erroneous phase shifts are combined together for the iterative corrections), though the reconstructed phase shift is one criterion for judging the accuracy of reconstructions.

7. SIMULATION RESULTS PLOTTED AGAINST $\Delta\psi/\pi$

This section will present and analyze a series of plots of various errors and improvement factors. The horizontal axis for all plots is the phase shift through the diameter of the lossless cylinder divided by π. The four curves are results of reconstructions for the fixed object sizes $k_o a$ = 4.7, 12.6, 32, and 46, corresponding to objects of radii 0.75, 2.0, 5.1, and 7.3 wavelengths. Each point on each curve represents the error or improvement factor for an individual run under conditions of the given object size and speed of sound contrast (phase shift). Let $\tilde{\gamma}^i$ designate the estimated object function after iteration i. The first plot, figure 10a, is the log of the squared error normalized to the number of pixels in the cylinder, $n_{\gamma\neq 0}$, after zero iterations. A given phase shift requires larger contrast values for smaller cylinder radii and therefore larger $|\gamma|$ (see Eq. (2)). The initial error E_0 is in fact the exact object function because the initial guess is zero; that is,

$$E_0 = \log_{10}\left(\frac{||0-\gamma^{ex}||^2}{n_{\gamma\neq 0}}\right) = \log_{10}\left(n_{\gamma\neq 0} \cdot \frac{(\gamma_{cyl}^{ex})^2}{n_{\gamma\neq 0}}\right)$$

$$= 2\log_{10}(\gamma_{cyl}^{ex}) \qquad (4)$$

where γ_{cyl}^{ex} is the value of γ^{ex} within the cylinder. Thus, the initial error will be higher for decreasing cylinder radii, and so the four curves are separated. In particular, $\Delta\psi = \pm\pi$ is achieved for speed of sound contrast (-25/50) percent for $k_o a$ = 4.7 and (-3.3/3.5) percent for $k_o a$ = 46. The same minimum contrast value was chosen for all sizes: ± 1 percent, so the normalized initial error is the same for all four sizes (note that the phase shift for ± 1 percent increases with object size). The minimum value of the curves follows from the value of γ for a 1 percent contrast cylinder:

$$\gamma_{1\%} = (2\pi \cdot 2)^2 \left(\frac{1}{1.515^2} - \frac{1}{1.5^2}\right) = -1.384 \left(\frac{rad}{mm}\right)^2 \qquad (5)$$

so $E_{min} = 0.282$ (> 0).

The next plot, figure 10b, is the same error after the first iteration, which is based on the Born approximation. Nearly the same relation between the curves is maintained as in the initial error plot (Fig. 10a). Improvement over the initial guess is limited to the cases where $|\Delta\psi| << \pi$, where E drops below zero (which here merely indicates that $\sum_{j=1}^{n^2} (\tilde{\gamma}_j^1 - \gamma_j^{ex})^2 < n_{\gamma\neq 0}$). Outside $\pm\pi$ the error is no lower than that of the initial guess.

Figure 10c shows the error after eight iterations. One can see dramatic improvements in the error vs. phase shift within $\pm\pi$; for a given phase shift the error curve is pulled down. In fact, the amount pulled down increases somewhat with object size, for intermediate sizes. However, the two $k_o a$ = 64 (101x101 grid) results obtained for four iterations are added as separate points to the plot, and, together with the $k_o a$ = 32 (55x55 grid) and $k_o a$ = 46 (75x75 grid) curves show that this trend does not

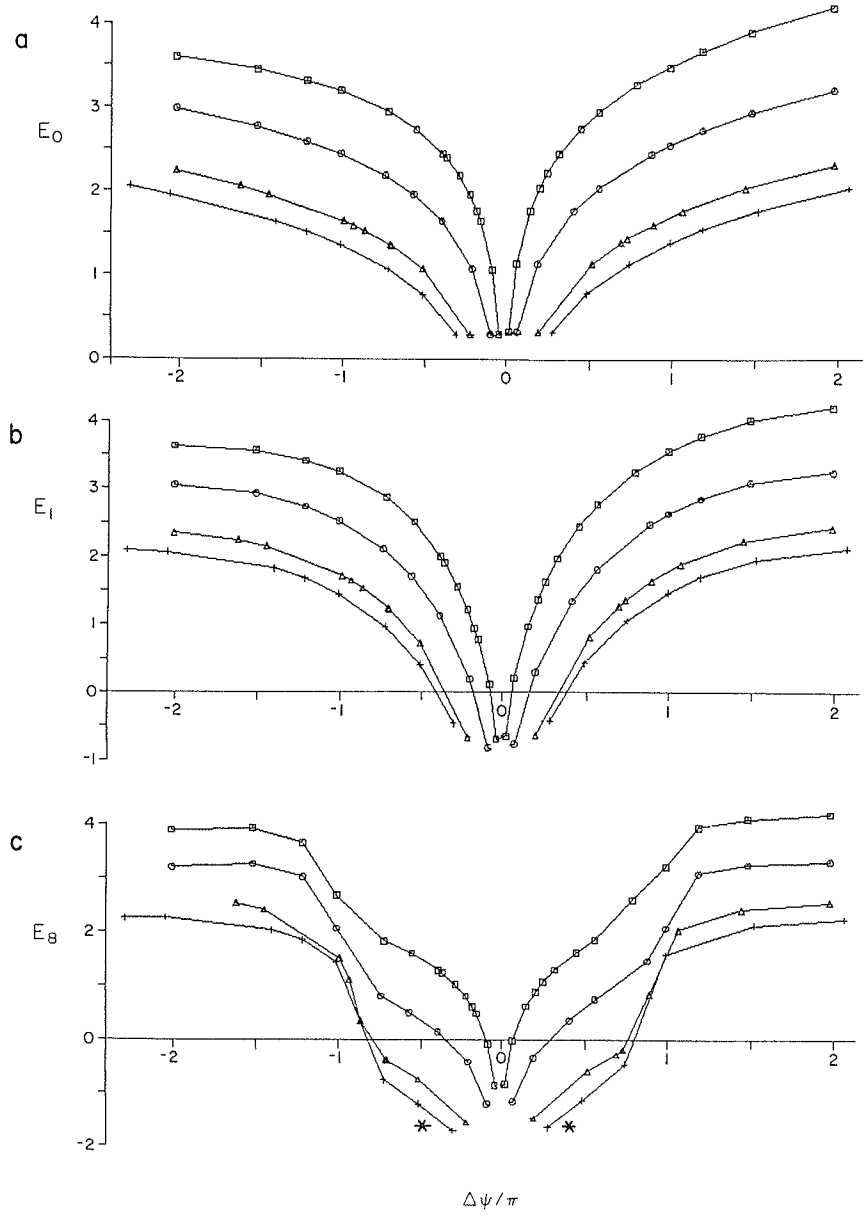

Fig. 10 Error after i = zero (a), one (b), and eight (c) iterations $E_i = \log_{10}\{||\tilde{\gamma}^i - \gamma^{ex}||^2/n_{\gamma\neq 0}\}$ vs. $\Delta\psi/\pi$ for five object sizes: $k_o a$ = 4.7 (□), 12.6 (o), 32 (Δ), 46 (+), and 64 (*) (only two runs, shown in (c) only).

continue for larger objects. Again, outside of $\pm\pi$ the error is no lower than that of the initial guess. In addition, shown as separate points are the results of the object size study of Section 5. Each of those points is

a 5 percent contrast cylinder of radius 17 through 10 pixels (left to right) reconstruction. As could be expected, the smaller sized cylinders have decreasing phase shift magnitudes for the fixed contrast, and consequently result in lower errors. The slight upturn in the error for the smallest few cylinders is due to the problem noted above of incomparability of results when using the same grid spacing for different problems. In an experimental setup, some estimate would have to be used for the minimum object component size likely to be encountered, in choosing the grid spacing. In addition, in figure 10c, the only two runs for which the 101x101 program version completed eight iterations ($\pm$1 percent) are plotted as separate points, and are found just below the $k_o a = 46$ curve. They again indicate that the situation, even within $\pm\pi$, will not indefinitely improve with increasing object size, even neglecting the problem of the enormously growing computational loads.

Figure 11a is a set of plots of $S_{01} = 10 \log_{10}(||0-\gamma^{ex}||^2 / ||\tilde{\gamma}^1-\gamma^{ex}||^2)$, the dB improvement in the squared error vs. $\Delta\psi/\pi$ after one iteration (the Born approximation) over the initial error. Note the relatively low dependence on object size--the curves are all close together. The closeness indicates that this one basic curve may represent a fundamental characteristic of the result of using the first Born approximation for tomographic reconstruction. There are improvements of up to 10 dB for very low contrast (1 percent), but outside of $\pm 0.85\pi$ the dipping below zero indicates a small degradation over the initial guess of zero for γ. Interestingly, the value of this degradation remains fairly constant for large ranges of $\Delta\psi$ outside $\pm\pi$.

Figure 11b shows the improvement factor in dB after 8 iterations, S_{08}, over the initial guess vs. phase shift increment. The encouraging feature here is that the improvement increases with object size, and is relatively flat within $\pm\pi$, peaking at near 20 dB, compared with 10 dB for the Born approximation. The flatness of the curves shows that when the assumptions of the algorithm are valid, the sinc basis method yields a solution whose improvement over the initial guess of zero is fairly independent of the phase shift through the diameter of the cylinder. Here, as $\pm\pi$ are approached from zero, additional limitations are found on performance as (roughly) $\pm 0.85\pi$ are reached. This phenomenon of beginning to fail slightly before $\pm\pi$ presumably results primarily from the poor initial guess for the internal field (the incident field), and possibly also from the discretization of the original integral equations, the sinc basis field representation, and other numerical errors. Again, because of the nonuniqueness problem occurring for phase shifts greater than π, the algorithm fails outside the region where the "minimum norm" solution as obtained by ART coincides with the desired solution.

It is interesting to note that while the Born approximation gradually deteriorates to approximately no improvement at $\pm$ 0.8π (Fig. 11a), the sinc basis method fails <u>abruptly</u> at approximately $\pm\pi$. This behavior indicates that the phase shift nonuniqueness problem is now the most serious limitation of the algorithm.

Figure 11c shows the improvement factor after 8 iterations over the first iteration (Born approximation), S_{18}, vs. phase shift:

$$S_{14} = 10\log_{10}\left(\frac{||\gamma^1 - \gamma^{ex}||^2}{||\gamma^8 - \gamma^{ex}||^2}\right) \qquad (6)$$

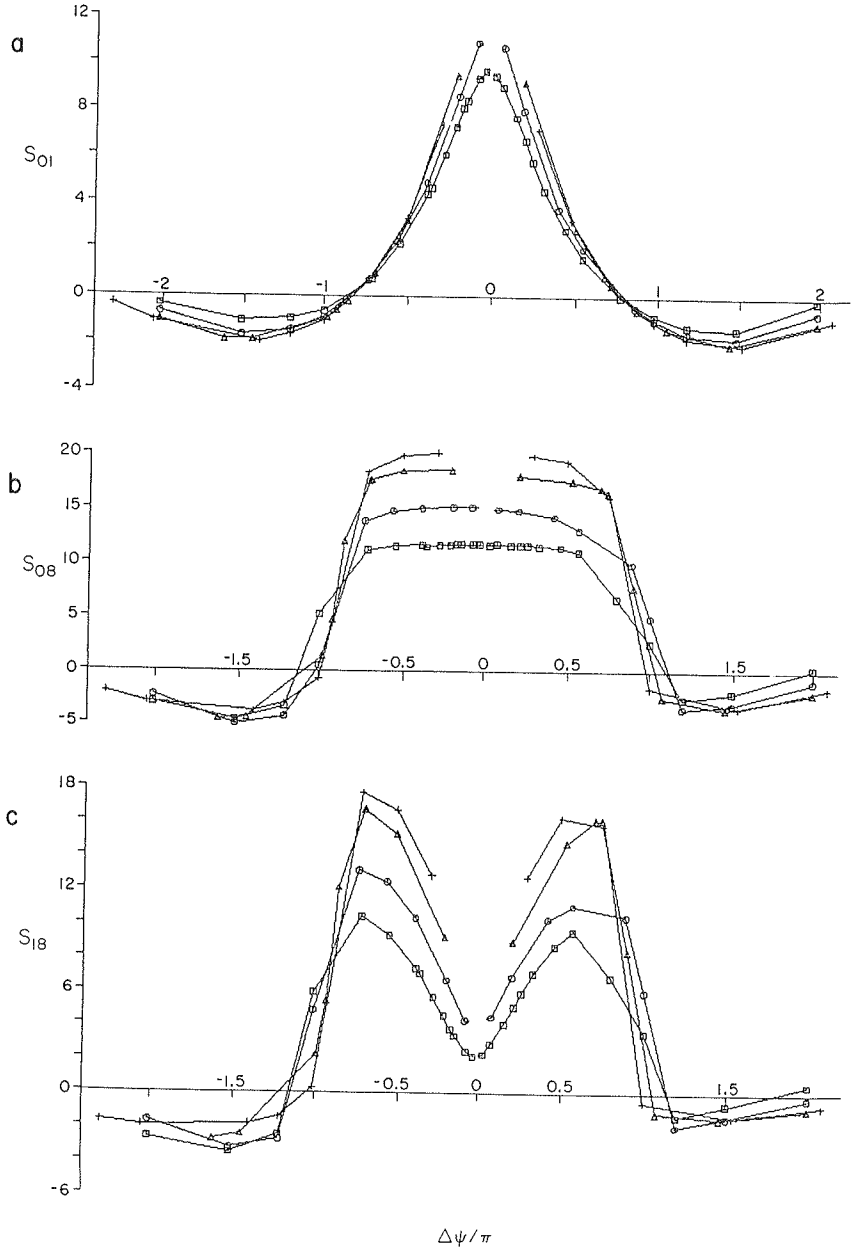

Fig. 11 Improvement factor, S_{ij}, in squared error of $\tilde{\gamma}$ after j iterations over the ith iteration for ij = 01 (a), 08 (b), and 18 (c), vs. $\Delta\psi/\pi$ for four object sizes: $k_o a$ = 4.7 (□), 12.6 (o), 32 (Δ), and 46 (+).

Because of the property of the log of a quotient, figure 11c represents the differences between the curves in figures 11b and 11a. For very small contrasts the Born approximation is already good, so the improvement factor is

small. The improvement factor steadily increases for increasing phase shifts to a peak of about 18 dB until $\pm\pi$ are approached, at which point the algorithm begins to fail. This increase is due to the increasingly poor Born solution occurring, while the improvement of the sinc basis method is relatively constant within this range of $\Delta\psi$. If the solution to the difficult problem of adding signals with unwrapped phases or other nonuniqueness-resolving techniques were known and could be applied here it is conceivable that the improvement factor could continue its increasing trend outside the $-\pi$ to π interval.

Figures 12a through 12c give the absolute value of the percent error in the initial estimated average speed of sound within the cylinder c_o, after 0, 1, and 8 iterations, normalized to the exact percent contrast.

The normalization was performed in order to remove the effect of bias in the curves for different object radii, stemming from the fact that for increasing object size, a given phase shift will have decreasing initial error in speed of sound estimation (see also the discussion concerning figure 10a). So, one would expect that by normalizing to the percent contrast one could at least partially make the curves uniform, and better represent a fundamental limitation of the present implementation of the sinc basis moment method. Figure 12a gives the absolute value of the initial percent error in the estimated speed of sound within the cylinder, divided by the percent contrast:

$$\left|\left(\frac{c_o-c_1}{c_1}\right) \Big/ \left(\frac{c_1-c_o}{c_o}\right)\right| = \left|\frac{c_o}{c_1}\right| \tag{7}$$

which is simply a set of linear curves. The curves intersect at $\Delta\psi = 0$, normalized error = 1, and the angle with respect to the horizontal increases with decreasing cylinder size, for the same reason given above.

Figure 12b gives the same error after one iteration:

$$\left|\left(\frac{c_1^1-c_1}{c_1}\right) \Big/ \left(\frac{c_1-c_o}{c_o}\right)\right| = \left|\frac{c_o(c_1^1-c_1)}{c_1(c_1-c_o)}\right| \tag{8}$$

where in general $\bar{c}_1^j$ is the average estimated speed of sound in the cylinder region after j iterations. Here, the reason for dividing by percent contrast is evident. In plots of the unnormalized percent error [4], the curves for different sizes are widely spread out because of the fact about percent contrasts vs. phase shift vs. size, given above. In figure 12b the curves are all close together, indicating a general behavior of the algorithm rather than merely various results for particular objects.

Finally, in figure 12c the same error for iteration eight is plotted:

$$\left|\left(\frac{c_1^8-c_1}{c_1}\right) \Big/ \left(\frac{c_1-c_o}{c_o}\right)\right| = \left|\frac{c_o(c_1^8-c_1)}{c_1(c_1-c_o)}\right| \tag{9}$$

There is a dramatic reduction in the percent error of estimated speed of sound within the cylinder for $|\Delta\psi| < \pi$. For example, at $\Delta\psi = \pm 0.7\pi$, the

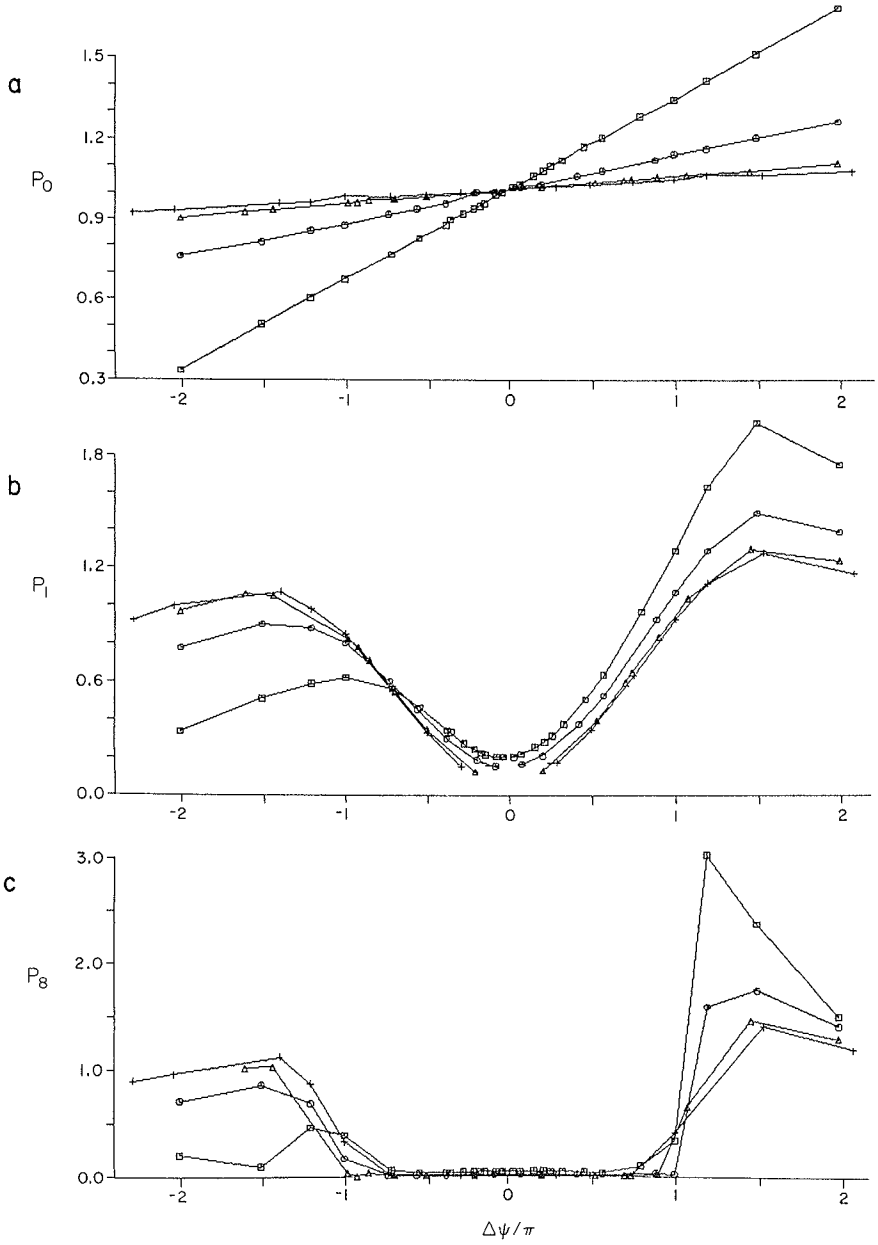

Fig. 12 Absolute value of the percent error, normalized to exact percent contrast, in the estimated speed of sound within the cylinder after zero iterations, P_i, for i = 0 (a), 1 (b), and 8 (c) vs. $\Delta\psi/\pi$ for four object sizes: $k_o a$ = 4.7 (□), 12.6 (o), 32 (Δ), and 46 (+).

magnitude of the error in estimated c_1 was less than 0.07 percent for all sizes, but for $\Delta\psi = \pm\pi$ that error jumps to more than 1 percent [4]. The uniformity among the curves for different radii is even more marked here if

the curve for the smallest cylinder ($k_0a = 0.75$) is removed, which for all cases is the curve off by itself (probably due to a high discretization error caused by using a small number of pixels to represent the circular shape of the object).

8. TISSUE CHARACTERISTICS

Typical range for speed of sound in human soft tissue are 1.46 mm/μs (fat) through 1.5 mm/μs (water) through 1.7 mm/μs (tendon) and for pressure absorption coefficient from near zero (water) up to 0.04 Np/mm/MHz (abdominal wall) [10]. A more typical value for insonification frequency than the 2 MHz used in this paper would be 5 MHz, which would accentuate the attenuation effects of absorption because of the power law dependence of absorption on frequency. Object size will depend drastically on the particular specimen being examined, but undoubtedly will be at least hundreds of wavelengths--a long way from the sizes that have been successfully reconstructed in this and other papers. In the previous section, it was noted that this reconstruction algorithm breaks down if the phase shift increment in the scattering object exceeds π. For a clinically realistic example, a cylinder of diameter 1000 wavelengths and speed of sound 1.7 mm/μs, the phase shift is about 235 π. Clearly, any practical implementation will have to somehow eliminate this phase shift problem, which exists for many other algorithms as well. One attempt at circumventing this problem was recently proposed [11]. That method is to successively solve again a reconstruction problem at increasing frequencies such that the maximum phase shift increment magnitude between the true solution and the current initial guess is always less than π. Note that later in the process, the initial guess (result from previous frequency solution) will have to be better and better to maintain initial error in the phase shift magnitude as less than π because the phase shift is proportional to the (increasing) frequency (Eq. (2)). It is not clear how this would be guaranteed under the proposed successive doubling of the frequency. In conclusion, the effects of the many required grid interpolations and the current practical inefficiency of obtaining so many precise single frequencies from a large array of transducers of limited bandwidths remain to be demonstrated.

9. USE OF ALTERNATIVE INITIAL GUESSES FOR γ AND f^{int}

9.1 Initial guess for γ is zero

In order to find out more about the nature of local solutions obtainable by ART with an initial guess of zero for γ and about the accuracy requirements for the field, a 25x25 grid speed of sound contrast study of lossless, $k_0a = 12.6$ circular cylinder reconstructions was performed that 1) compared reconstruction quality for three field conditions as outlined below and 2) used symmetrical about zero values of $\Delta\psi/\pi$ as the independent variable [4]. An example of the composites of this study is shown in figure 13 which shows negative phase shift speed of sound reconstructions for iterations 9 and 12, all plotted against the exact solution. In the leftmost and middle columns of the composite, respectively, the incident field and exact internal field [6] are used as the initial guess for the internal field. Also in these columns, both internal and scattered field matrix equations [3] are used, as usual, to solve for better estimates of both γ and the internal field. In the rightmost column, the exact internal field is used as the internal field estimate for <u>all</u> iterations (no iterative corrections on the field are performed).

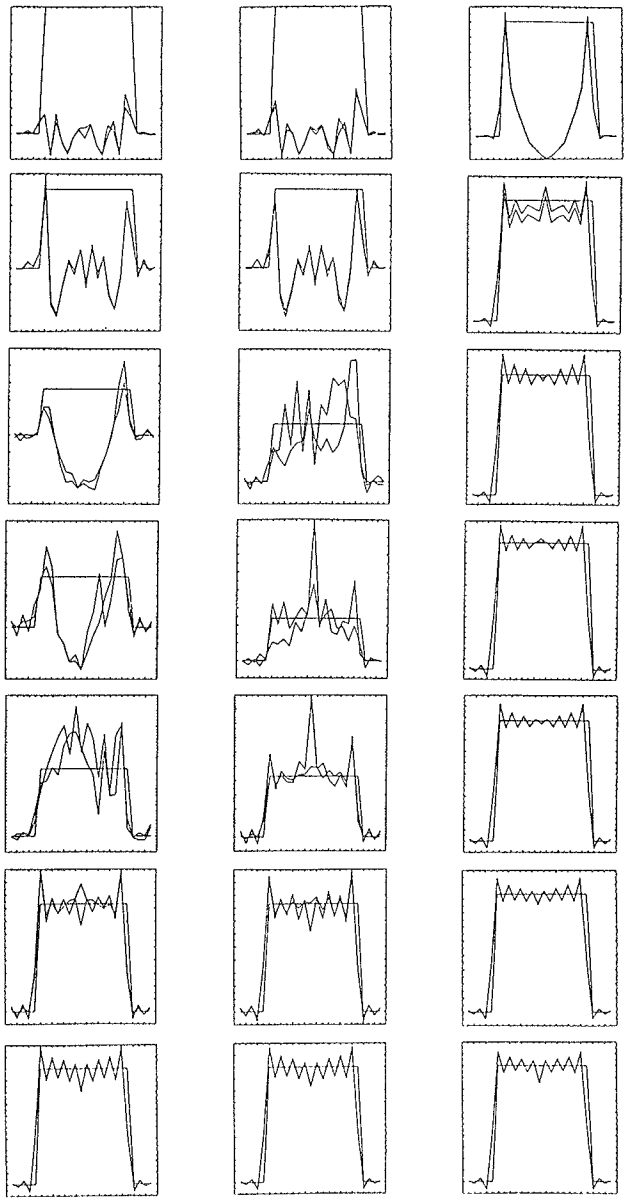

Fig. 13 Center-line profiles of ninth- and twelfth-iteration speed of sound reconstructions and exact solution for lossless, $k_0a = 12.6$ cylinders. Variation of reconstruction quality with phase shift $\Delta\psi$ through the cylinder. From top to bottom, phase shifts for all three reconstructions on each row are: $\Delta\psi/\pi$ = -4.0, -2.0, -1.2, -1.1, -1.0, -0.8, and -0.5. Initial guess for the internal field is the incident field (left column) and the exact internal field (center and right columns). Iterative improvements are made on the internal field estimation in the left and center columns, but not on the right. Straight-line distributions are exact solution. Where visibly differing, the curve close to the exact solution is the twelfth iteration, and the remaining curve is iteration nine.

First consider reconstructions in the leftmost column. As expected from previous studies, when using the incident field as the initial guess for the total internal field, the algorithm succeeds for low contrast cases ($\Delta\psi/\pi$ = -0.5 and -0.8), but breaks down for phase shift magnitude greater than π. Note, however, that the $-\pi$ reconstruction is on the threshold of having a cylinder shape with an acceptable average speed of sound. Note also that in the vicinity of $-\pi$ ($-\pi$, -1.1π, and -1.2π) that these reconstructions are most asymmetrical, and changing with iteration even after 9 iterations. Very large phase shifts (-2π and -4π) show a return to stability, but on an erroneous solution (with phase shift magnitude less than π).

Now consider the middle column, where the exact internal field was used as the initial guess for the internal field. For $|\Delta\psi|<\pi$, the final reconstructions are about the same as those using the incident field, but convergence is attained a few iterations sooner [4]. In the vicinity of $-\pi$ ($-\pi$, -1.1π, and -1.2π) the asymmetrical behavior is actually accentuated compared with that in the leftmost column, though the reconstructions for using the exact internal field are decidedly more accurate. In fact, the reconstructions for $|\Delta\psi| = \pi$ are actually fairly acceptable as quantitative estimates of the speed of sound within the cylinder (especially the average). Comparison of iteration 1 of the leftmost and middle columns [4] shows a dramatic improvement resulting from using the exact field over using the incident field for all phase shifts having magnitude up to 1.2π. For $|\Delta\psi| = 2\pi$ and 4π, however, the reconstructions for all iterations in these two columns are nearly identical, and settle upon erroneous estimated object functions.

The rightmost column is unique in that the internal field is held fixed at its initial value, namely the exact internal field, for all iterations. In fact, higher iterations can be considered as various stages in one long iteration over the scattered field equations. Very high quality reconstructions are obtained for phase shift magnitude up to 1.2π. What is most remarkable, though, is the (very slow but definite) convergence after 12 iterations for the case $|\Delta\psi| = 2\pi$! It is currently not known why convergence to the correct solution was obtained for this case; it does not neatly fit the theory proposed in earlier sections. One possibility may be that there simply <u>is</u> no local solution having phase shift magnitude less than π, in this case. Further study could investigate this question; however, the question is merely academic, as in no practical setting will the exact field be known beforehand. Furthermore, for $|\Delta\psi| = 4\pi$ the solution in the third column is finally stable and erroneous, although of a different shape from that of the other two columns.

Finally, an aspect supportive of earlier statements that $\Delta\psi$ is fundamental in determining performance is clearly supported in this study. Especially notable is the strong comparability of reconstruction quality between reconstructions of cylinders having phase shifts of equal magnitude and opposite sign [4]. In fact, all of the statements above are valid for both signs of phase shift having the specified magnitude. Also, it can be concluded from the failure of the algorithm for large $\Delta\psi$ when using the exact internal field that it is not the large error of the Born approximation that fundamentally limits performance of the sinc basis moment method, but rather the phase shift nonuniqueness problem described earlier in Section 6 and other factors. It also can be concluded that although high accuracy in the estimation of the internal field is indeed crucial for successful reconstruction it is obtainable within a few iterations, at least for low magnitude phase shift problems [3].

9.2 Initial guess for γ is close to γ^{ex}

In figure 14 is a composite showing iterations 9 and 12 (earlier iterations are similar) of a $k_o a = 12.6$, -27.2 percent speed of sound mismatch lossless cylinder ($\Delta\psi/\pi = 3.00$) under the following conditions. In the left column the initial guess for the internal field was the incident field, and the internal field sinc basis expansion equations were used in the iterations to improve that estimation, while in the right column the exact internal field was used as the internal field estimation for all iterations (no iterative corrections were made on the field). In the top row the initial guess for γ was zero; that is, the speed of sound was assumed to be c_o everywhere within the object region. In lower rows, the initial guess for the speed of sound (i.e., through $\tilde{\gamma}$) was a cylinder of the exact shape and size of γ^{ex} but with the guess for the speed of sound within the cylinder, $\tilde{c}_1^0$, increasingly accurate for lower rows: 37.5 percent error (first row); 10, 5.4, 2.7, and 0.0001 percent error (bottom row). For the case of using the exact internal field, the algorithm settles on an erroneous solution for $\tilde{c}_1^0 = 1.5$ mm/μs ($= c_o$), but gradually improves further down the composite to where the nearly perfect match at the bottom stays nearly perfect. Note that for the lower rows the solution only bends around $\tilde{c}_1^0$, and does not converge to c_1. There appear to be multiple weak local solutions highly dependent on $\tilde{c}_1^0$ for this high contrast case, which is unfortunate because it means that the initial guess must be very good to begin with, and then only minor improvement, if any at all, occurs from there. Regardless, as mentioned in the preceding subsection, knowledge of the exact internal field (let alone knowledge of the exact object shape) will not be available in a practical setting.

The situation is even worse in the left column, where the incident field is used as the initial guess for the field. All solutions are highly erroneous, even the one in the bottom row, for which the initial error in speed of sound in the cylinder was only 0.0001 percent. Perhaps it is this figure which is most disturbing for prospects for any future practical use of the sinc basis method, at least without some major basic improvements such as use of unwrapped phase in some way, or constraints as yet not applied to the iterating field and object function estimates. One additional further improvement that might be interesting to try would be use of the Rytov solution, as the initial guess for γ. However, as shown above, even a very good initial guess for the object function will immediately be corrupted if a poor estimate such as the incident field--the only one available--is used for the total internal field, so it probably would not be worth the effort. It should be mentioned that for all reconstructions in this work, an additional simplification concerning correction of the internal field was used [3]. The assumption behind it was dependent on weak scattering; further studies will relinquish this simplification to see if the above behavior with respect to the internal field can be improved.

10. LOSSY CYLINDER RECONSTRUCTIONS

With the availability of a complex Bessel function routine, it was possible to modify the scattered field generator program to calculate scattered fields from lossy cylinders. Depending on the magnitude of the absorption coefficient, loss in a sense minimizes multiple scattering effects because scattering that was, for the lossless object case, weak in the object region in a particular direction is with loss even further reduced in magnitude. Computationally, in the reconstructions this effect is manifested in a complicated way, through the matrix coefficients, incident field, and modified scattered field (compared with the corresponding

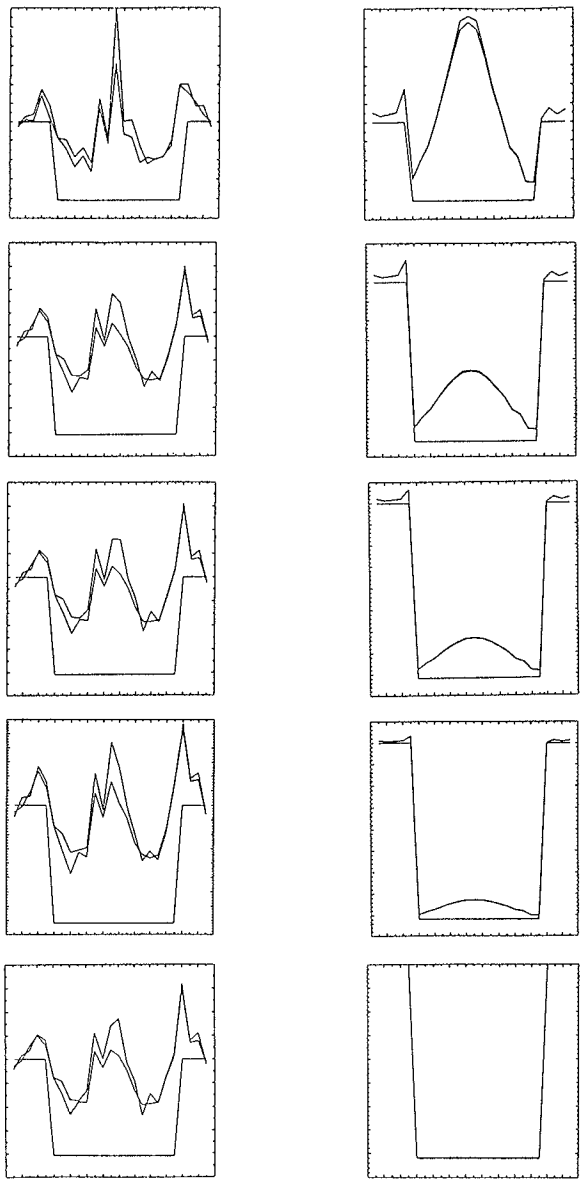

Fig. 14 Center-line profiles of ninth- and twelfth-iteration speed of sound reconstructions and exact solution for a lossless, $k_o a = 12.6$ cylinder having speed of sound 1.090909 mm/μs. Variation of reconstruction quality with initial guess for speed of sound within the cylinder. From top to bottom, $\tilde{c}_1^0 = 1.5$, 1.2, 1.15, 1.12, 1.09091 mm/μs. All reconstructions in left column are for the case of using the incident field as the initial guess for the internal field; all those in the right column are for the case of using the exact internal field for all iterations (no iterative corrections on the internal field estimation). Straight-line distributions are exact solution. Where visibly differing, the curve close to the exact solution is the twelfth iteration, and the remaining curve is iteration nine.

lossless case), which determine a modified estimated γ: first as estimated through the scattered field equations and then indirectly through a modified estimate of the field obtained from the internal field equations. For a complete set of composites for this study, see [4].

First, the speed of sound was varied for a $k_o a = 12.6$ cylinder while the pressure absorption coefficient was held constant at the high value of 0.2 Np/mm at a frequency of 2 MHz. The speed of sound percent contrasts were varied between -5 and 13.3. As the speed of sound increased, the real part of the exact object function ranged from 2.1 to -5.3 times its imaginary part. In spite of this, the speed of sound and absorption reconstructions both begin to be slowly converging and unacceptable at about the same level of speed of sound contrast--that for $|\Delta\psi|$ approaching π.

Next (Fig. 15), the speed of sound contrast was held constant at +5 percent while the pressure absorption coefficient was varied as follows: 0, 0.1 Np/mm, 0.4 Np/mm, 0.7 Np/mm, 1.0 Np/mm. Here a different behavior was observed: when the speed of sound reconstruction fails, the absorption reconstructions are still quite good after five and especially after eight iterations. Several factors are influencing this behavior. The norm of the object function is increasing and consequently, so is the contribution of the object function to the widening of the object function-total field spectrum, whose width determines the estimated Nyquist sampling density [3]. Also, the initial guesses for the object function and the internal field are increasingly worse. However, the phase shift problem should not be present because absorption mismatches vary amplitudes, not phases, and the phase shift magnitude through all these cylinders is far less than π--only 0.4π. The value of the imaginary part of γ (containing object absorption and speed of sound as factors) is twice that of the real part (containing only object speed of sound) for the bottom row reconstruction in figure 15. However, the absorption reconstruction is slowly closing in on the desired solution while the the speed of sound reconstruction has settled on an erroneous solution. Therefore, speed of sound reconstructions may be more fundamentally limited than low speed of sound-mismatch absorption reconstructions, although in reality such factors as signal-to-noise ratio and others may dominate.

Next, the speed of sound was set to c_o, a perfect match with the coupling medium, to examine the behavior of absorption reconstructions without including any phase shift effects. Results were similar when not superior to those of figure 15, which had the same absorption values but a 5 percent speed of sound mismatch. Again, for very high absorption values the reconstruction process becomes slow and accuracy steadily diminishes, but these absorption values are larger than those that would be found in soft tissue, even at substantially higher frequencies within the diagnostic range. And under conditions of a perfect speed of sound mismatch, perhaps object size would not be such a limiting factor, at least not theoretically by the phase shift requirement.

Finally, the absorption was held a perfect match with the coupling medium, zero, while the speed of sound mismatch was again varied from -5 to 13.3 percent. Here one finds that, for the same magnitude in object function, the speed of sound reconstructed cylinder shape is far worse than for that of the maximum contrast absorption reconstruction with matched speed of sound. There occurred an erroneous cylinder shape in the first iteration of the absorption reconstruction (see [3]), which should be zero;

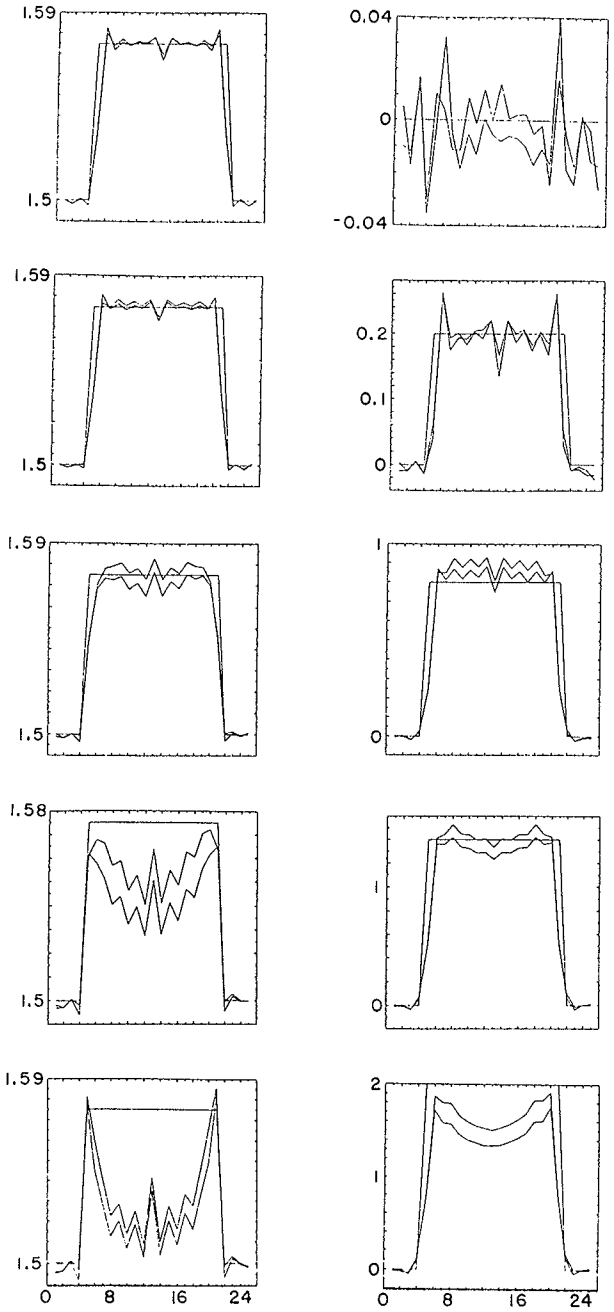

Fig. 15 Center-line profiles of fifth- and eighth-iteration speed of sound (left) and absorption (right) reconstructions and exact solutions for 5 percent speed of sound mismatch ($\Delta\psi = 0.4\pi$), $k_o a = 12.6$ cylinders. Variation in object reconstruction quality with pressure absorption coefficient: $\alpha_1 = 0$, 0.1 Np/mm, 0.4 Np/mm, 0.7 Np/mm, 1.0 Np/mm. Straight-line distribution is exact solution, curve closer to exact solution is iteration eight, and remaining curve is iteration five.

but for the matched speed of sound case the Born approximation yielded speed of sound profiles which oscillated about the exact solution.

A general conclusion from this study might be that in the case of weak scattering, performance of speed of sound and absorption reconstructions are comparable, but because absorption contrast does not contribute to phase shifts while speed of sound contrast does, the algorithm will converge for stronger contrast and presumably larger size absorption objects than speed of sound mismatch objects. Of course in reality, both speed of sound and absorption contrasts will be significant. Note that for a lossy (0.02 Np/mm), very high speed of sound contrast cylinder ($\Delta\psi/\pi$ = 3.0), both speed of sound and absorption reconstructions failed. Thus, the phase shift problem destroys both speed of sound and absorption reconstruction quality.

11. CONTRIVED OBJECT

For the sake of investigating reconstruction quality for a more complicated object, a superposition of three simple lossy shapes was chosen. The values for c_1 and α_1 and sizes were chosen as shown in table II. The largest phase shift, through the diagonal of the rectangle, was consequently -0.3π, well within the range for successful reconstruction of cylinders. Of course, no exact solution was available for this multiple scattering problem, so the internal field equations were used to solve for the internal field, and then it and the exact γ were used in the measured scattered field equations to generate the scattered field. (A cylinder spatially shifted from the center of the object region was successfully reconstructed using exact scattered fields [4]. That such reconstructions were just as accurate as those for an equivalent centered cylinder additionally indicates that the validity of the algorithm is independent of the existence of object circular symmetry.)

The results for the contrived object reconstructions are shown in figure 16; the exact γ in the upper row and the fourth iteration reconstruction in the bottom row. On the left are speed of sound distributions, and on the right, absorption. The reconstruction is quite close to the exact solution in appearance, and is also numerically accurate, as the centerline profiles in figure 17 indicate (speed of sound in figure 17a and absorption in figure 17b), where in addition the first iteration has been included. Note that the behavior of the first iteration (first Born solution) is similar to that for the circular cylinder reconstructions; the reconstructed speed of sound is too close to c_o, while the absorption reconstruction has an erroneous shape, which mimics that of the exact speed

Table II. Parameters of Contrived Phantom

shape	c_1(mm/μs)	α_1(Np/mm)	size (wavelengths)
smaller cylinder	1.485	0.16	0.75 (diameter)
larger cylinder	1.515	0.32	1.50 (diameter)
rectangle	1.575	0.23	3.0x1.5

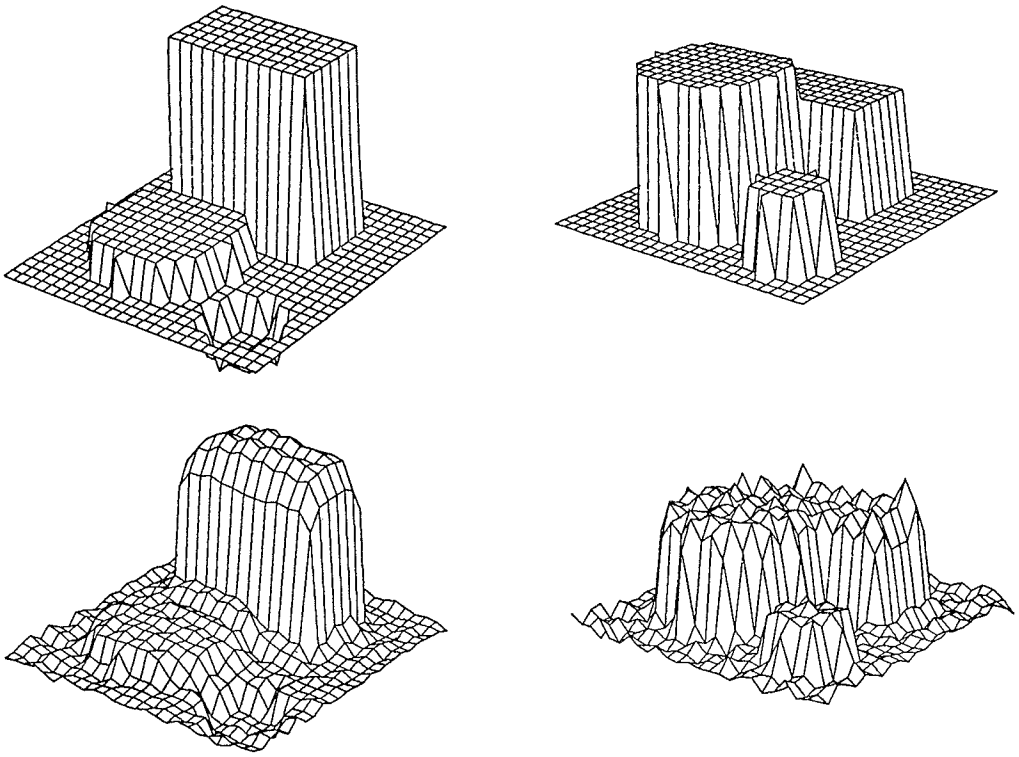

Fig. 16 Contrived object. Three-dimensional perspective views of speed of sound (left) and absorption (right) distributions. Exact solution (above), and fourth iteration reconstruction (below). For parameter values, see Table II.

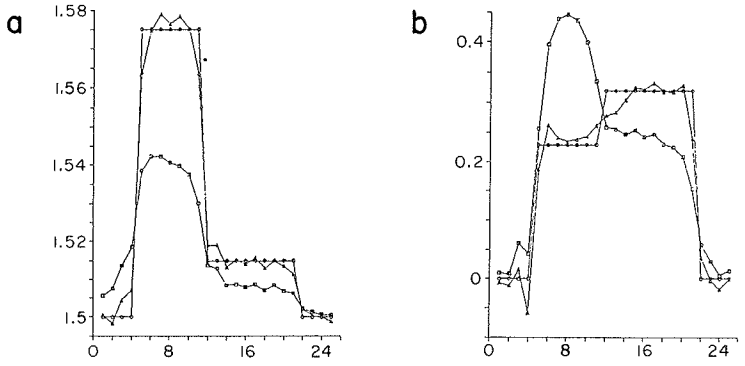

Fig. 17 Same contrived object as in figure 16. Cross-sectional line profiles of speed of sound (a) and absorption (b) distributions. Straight-line distribution is exact solution, curve closer to exact solution is iteration four, and remaining curve is iteration one.

Table III. Execution Times for the Sinc Basis Moment Method on Alliant Minisupercomputer vs. Grid Size

n_{max}	4 iters.	8 iters.
11	4 sec	8 sec
25	33 sec	74 sec
55	8 min	18 min
75	40 min	72 min
101	1hr, 40 min	3hr, 12 min

of sound distribution. The fourth iteration, however, oscillates about the exact solution. Raising the phase shift through the diagonal of the rectangle above π failed, as would be predicted from the discussions in Section 6.

12. EXECUTION TIMES

Table III summarizes execution times for four and eight iterations of the sinc basis moment method performed on the Alliant supercomputer. Those values are a far cry from the initial reconstructions on the VAX where an 11x11 reconstruction took 17 hours! There is a strong matching of the n^4 computational complexity dependence [7]. At present, grid sizes are limited to 101 x 101 (for a maximum object radius of over eight wavelengths) on the Alliant FX/8. (For an example of a low contrast 101 x 101 reconstruction, see [4].) Computation time and storage requirements remain formidable limitations of this algorithm in its present form, even when incorporating the FFT for a large fraction of the calculations [7].

13. SEQUENCE OF CONTROLLED EXPERIMENTS

A series of simulated controlled experiments was performed for which a single parameter or condition was modified from experiment to experiment (detailed tables from these simulations appear in [4]). All runs were reconstructions of lossless, $k_o a = 12.6$ circular cylinders. Parameters varied were initial guesses for γ ($\tilde{\gamma}^o$) and for the internal field, the method for scattered field generation, the relaxation parameter β_1 for orthogonal projections for the scattered field equations [3], the number of measurements (controlled by the number of detectors), and the speed of sound contrast. Let E_i^{ex} denote the squared error in $\tilde{\gamma}$ compared with γ^{ex} (the desired "exact" solution) after i iterations, ΔE_{01}^{ex} represent the change in E_i^{ex} from iteration zero (initial guess) to iteration one (Born approximation-based solution), and L_i^{ex} and L_i^{QR} denote the complex normalized inner products of the ith estimate of γ with respectively, γ^{ex} and γ^{QR} (two vectors in the same hyperdirection will have complex normalized innerproducts of one and orthogonal vectors, zero). Note that for this problem, $||\gamma^{QR}|| = 32||\gamma^{ex}||$ and the complex normalized product of γ^{QR} with γ^{ex} is only 0.03. For the first experiment, the speed of sound

contrast was 5 percent ($\Delta\psi = -0.4\pi$), the initial guess for both γ and the internal field was the true solution, and the scattered field was generated by using the sinc basis expansion equations. Obviously $E_0^{ex} = 0$, and because the scattered field is a perfect match with the sinc basis equations, E_1^{ex} also is zero. Due to discretization errors in the internal field equations (the incident field was not generated by the sinc basis equations and therefore is not a perfect match), E_2^{ex} is not zero, but rather 7.6. This error is, however, quite small relative to the initial error, and by iteration 4 it has grown to only 1/17 of the norm of γ^{ex}. If the series solution scattered field is used as input to the algorithm, the results are comparable, but now $E_1^{ex} = 37.4$ instead of zero. If $\tilde{\gamma}^o$ is changed to be zero, for this weak scattering case the estimate becomes quite close to γ^{ex} after four iterations. Actually, by far the greatest improvements in $\tilde{\gamma}$ are made during iteration 1. If the number of equations (just over twice as many measurements as unknowns) is halved, E_4^{ex} increases by a factor of three, but the reconstruction quality is still acceptable. In general, if the ratio of the number of measurements to number of unknowns is 1.1 or higher, reconstructions are acceptable; if lower than 1.0, they are far from acceptable even after nine iterations. If the initial guess for the internal field is changed to the incident field, the improvement during the first iteration is reduced, but by iteration 4 the estimated γ is almost as good as for using the exact internal field. If β_1 is varied, reconstruction quality varies such that $\beta_1 = 0.2$ is roughly optimum, though the optimal value is slightly problem dependent. A low optimum β_1 indicates that measurement values are not to be fully trusted, and corrections based on them will not be full orthogonal projections in magnitude; again (in the absence of additive noise) an indication of the discretization error in the sinc basis expansion equations. Increasing the speed of sound contrast to 10 percent ($\Delta\psi = -0.7\pi$) indicates why examining only the magnitude of the complex normalized inner product is insufficient to ascertain reconstruction quality. Although $|L_1^{ex}|$ is approximately one, the real and imaginary parts of L_1^{ex} are 0.48 and 0.8, respectively, and ΔE_{01}^{ex} is only 14 percent of E_0^{ex}. Thus, both real and imaginary parts of L_i^{ex} must be examined in using this indicator for a performance measure. If the field is held fixed at the initial guess of the incident field (iteration only on the scattered field equations), the squared error in γ after four iterations is fourteen times that after four iterations where corrections to the field are made, and even exceeds the error after one run through only the scattered field equations. This experiment verified the efficacy of the alternating variables aspect of this method. If the rows in the scattered field equations are reordered to maximize adjacent row orthogonality, there is no improvement gained despite huge computational expense. This is because the original adjacent placement of real and imaginary equations (representing one complex equation) already places together two rows that are exactly orthogonal [4] (real and imaginary row vectors), and subsequent rearrangement of complex equations has minimal effect. For the remaining experiments except the last, the internal field was set equal to the exact internal field (series computed) and the exact scattered field was used. All that is varied is the initial guess for γ. If γ^{ex} is used, $\tilde{\gamma}$ moves slightly away from γ^{ex} and toward γ^{QR}, presumably because γ^{QR} is the true mathematical solution; however, this movement, as noted above, is very slight. If the arithmetic average of γ^{ex} and γ^{QR} is used, the reconstructions are poor and $L_0^{ex} \simeq 0$ while $L_0^{QR} \simeq 1$ because $\tilde{\gamma}^0$ is very near γ^{QR} in a directional sense, due to the fact that $||\gamma^{QR}|| \gg ||\gamma^{ex}||$. To put $\tilde{\gamma}^0$ midway between γ^{ex} and γ^{QR} in a directional sense, the initial guess $1/2((||\gamma^{QR}||/||\gamma^{ex}||)\gamma^{ex} + \gamma^{QR})$ was used. Then $L_0^{ex} \simeq L^{QR}$ and $\Delta E^{ex} \simeq \Delta E^{QR}$ and the long-term behavior is not toward either γ^{ex} nor γ^{QR}, but is governed by the internal field corrections. If $\tilde{\gamma}^0$ is placed in a hyperdirectional sense 90 percent towards γ^{ex} and 10 percent towards γ^{QR}, $|L_0^{ex}| \simeq 0.99$ and $|L_0^{QR}| \simeq 0.14$. The squared error is reduced, but L^{ex} is

not maximized. Both E^{ex} and $|L^{ex}|$ may simultaneously decrease. If $\tilde{\gamma}^0$ is placed 90 percent towards γ^{QR} and 10 percent towards γ^{ex}, $\tilde{\gamma}$ moves toward γ^{ex} and away from γ^{QR} in terms of E_i, yet $\tilde{\gamma}$ is much closer to γ^{QR} innerproductwise than to γ^{ex}. It is evident that neither E nor $|L_i|$ tell the complete story about reconstruction quality, but in conjunction give a variety of indications. If $\tilde{\gamma}^0 = \gamma^{QR}$, $\tilde{\gamma}$ stays at γ^{QR} until the field estimation is modified. If a unit vector of magnitude $||\gamma^{ex}||$ at the location of either maximum or minimum $|\gamma^{QR}|$ is used for the initial guess for γ, $\tilde{\gamma}$ moves toward γ^{ex}; the behavior is actually not much different from using $\tilde{\gamma}^0 = 0$. If $\tilde{\gamma}^0 = 2\gamma^{ex}$, the error $E_1{}^{ex}$ is approximately the same as that obtained for $\tilde{\gamma}^0 = 0$, even though L_0 for the two cases is, respectively, 1 and 0, that is, as far apart as is possible for normalized inner products, again indicating the insufficiency of either E or L to completely characterize performance. Finally, for the last experiment, the initial guess for the internal field was reset to the incident field to better mimic a practical situation, and the initial guess for the speed of sound within the cylinder was chosen to be halfway between c_o and c_1. The result was indistinguishable from that for the case $\tilde{\gamma} = 0$.

14. CONCLUSION

To advance in high resolution ultrasonic imaging, two paths may be followed. One path, that of the perfection of B-scan systems, is actively being pursued by corporations currently involved in the production and marketing of such systems. Although quantitative distributions of physical ultrasonic parameters are not available from these echo images, high resolution, real time scanners with many features are currently in use. The other path involves using the techniques of inverse scattering to ascertain quantitative estimations of the induced sources within the tissue of interest which result from the interaction of selected incident ultrasonic waves with the tissue inhomogeneities. The currently available first-order algorithms are not only often difficult to implement, but are severely restricted in the range of problems they can approximately solve. Consequently, although the quantitative images obtainable from these methods would be very useful in making the body of knowledge of tissue characterization more useful in medical diagnosis, there are no commercially available systems precisely because of these restrictions on range of applicability of the algorithms as well as their high computational complexity. One method with more promise than first-order diffraction tomography algorithms is the sinc basis moment method. Because of its iterative, coupled equations form, and its fidelity to the exact integral equations (given the discretization/sinc basis expansion modifications), higher-order solutions are possible, and have been shown to be significant improvements over a typical first-order (Born approximation-based) inversion method reconstruction. However, the reconstructions obtained by the sinc basis moment method are again valid over only an unrealistically narrow range of problems. Although the order of complexity has been reduced significantly [7], it is still a very slow algorithm, and also has very large storage requirements.

These limitations of storage and speed are, however, of secondary importance in the long run, with the advent of ever faster and larger computers. It is the physical limitation concerning phase shift identified in this paper that needs immediate attention if the sinc basis method is ever to be seriously considered as a practical way of obtaining useful medical images. The basic area of signal processing of unwrapped phase signals (such as addition, with the constraint of commutativity) might be a good

place to start. Because unwrapped phase signals are noise-sensitive and difficult to obtain reliably, even progress in the theoretical side is no guarantee of the possibility of developing a practical, working system. But even if a tomographic system using this method is not practical, perhaps other uses for this formulation may be helpful in areas of field computations such as in hyperthermia research, where field distributions coupled with the bioheat equation could conceivably result in predicted temperature distributions in a given insonified tissue.

15. ACKNOWLEDGEMENTS

This work was supported by a grant from NIH (CA36029) and the Radiation Oncology Training Program (CA 09067). Dr. Michael J. Haney of the University of Illinois Center for Supercomputing Research and Development is gratefully acknowledged for access to the Alliant FX/8. Careful reviews of this paper by the peer reviewers are greatly appreciated.

REFERENCES

[1] Sehgal, C.M. and Greenleaf, J.F., Scattering of ultrasound by tissues, **Ultrasonic Imaging 6**, 60-80 (1984).

[2] Johnson, S.A. and Tracy, M.L., Inverse scattering solutions by a sinc basis, multiple source moment method - Part I. Theory, **Ultrasonic Imaging 5**, 361-375 (1983).

[3] Cavicchi, T.J., Johnson, S.A., and O'Brien, Jr., W.D., Application of the sinc basis moment method to the reconstruction of infinite circular cylinders, **IEEE Trans. Ultrasonics, Ferroelectrics, Freq. Control 35**, 22-23, 1988.

[4] Cavicchi, T.J., Diffraction Tomography and the Sinc Basis Moment Method, Ph.D. thesis, University of Illinois (1988).

[5] Lawson, C.L. and Hanson, R.J., **Solving Least-Squares Problems** (Prentice-Hall, Englewood Cliffs, NJ, 1974).

[6] Cavicchi, T.J. and O'Brien, Jr., W.D., Acoustic scattering of an incident cylindrical wave by an infinite circular cylinder, **IEEE Trans. Ultrasonics, Ferroelectrics, Freq. Control 35**, 78-81, 1988.

[7] Cavicchi, T.J. and O'Brien, Jr., W.D., Convergence and speed of the sinc basis moment method, in **1987 IEEE Ultrasonics Symposium**, pp. 907-910, (IEEE Cat. No 87CH2492-7).

[8] Mueller, R.K., Kaveh, M., and Wade, G., Reconstructive tomography and applications to ultrasonics, **Proc. IEEE 67**, 567-587 (1979).

[9] Pan, S.X. and Kak, A.C., A computational study of reconstruction algorithms for diffraction tomography: interpolation vs. backpropagation, **IEEE Trans. Acoust. Speech, Signal Proc. ASSP-31**, 1262-1275 (1983).

[10] Goss, S.A., Johnston, R.L., and Dunn, F., Comprehensive compilation of empirical ultrasonic properties of mammalian tissues, J. Acoust. Soc. Amer. 64, 423-457 (1978).

[11] Kim, W.W., Borup, D.T., Johnson, S.A., Berggren, M.J., and Zhou, Y., Accelerated inverse scattering algorithms for higher contrast objects, in **1987 IEEE Ultrasonics Symposium**, pp. 903-906, (IEEE Cat. No. 87CH2492-7).